Oceanologia 64 (2022) 299—311

Available online at www.sciencedirect.com

ScienceDirect

journal homepage: www.journals.elsevier.com/oceanologia

ORIGINAL RESEARCH ARTICLE

Diurnal variation of cloud cover over the Baltic Sea

Marcin Paszkuta[a,*], **Tomasz Zapadka**[b], **Adam Krężel**[a]

[a] *Institute of Oceanography, University of Gdańsk, Gdynia, Poland*
[b] *Institute of Physics, Pomeranian University in Słupsk, Poland*

Received 3 January 2021; accepted 13 December 2021
Available online 29 December 2021

KEYWORDS
Clouds;
Baltic Sea;
Environmental assessment

Abstract Instantaneous cloud cover over the Baltic Sea, estimated from satellite information, may differ by as much as several dozen percent between the day and night. This difference may result from both weather conditions and different algorithms used for the day and night. The diurnal differences in cloudiness measured by proprietary and operational systems were analysed as part of research on marine environmental assessment and monitoring. An optimised algorithm for 2017 was presented and supplemented with information from radiation modelling. The study showed that, in general, the average values of daily changes in cloud cover over the sea depend on the season, which generally corresponds to the length of the day and contrasts with the amount of cloudiness. The results were compared with available online data that met the night and day detection criteria, the climate model, and the climate index. The averaged analysis of seasonal changes showed that similar values of the satellite estimates are higher than those obtained from the climate model and the lidar estimation. The satellite estimates from SatBaltic showed the lowest uncertainty. The diurnal cycle was confirmed by all analysed systems. These results may indicate common physical mechanisms and a methodological reason for the uncertainty of satellite-based data. The results clearly showed the existing diurnal difference in the amount of cloud cover over the Baltic Sea and indicated that this difference is not always explained by the physical properties of the atmosphere. The probable causes for these uncertainties were identified and diagnosed.

1. Introduction

The study of cloudiness above the sea surface based on observations from satellites is a very complex problem. The complexity involves results of measurements in both the shortwave and longwave ranges, i.e. the visible (VIS) and infrared (IR) radiation. The literature includes numerous studies (Anthis et al., 1999; Bennouna et al., 2010; Finkensieper et al., 2018; Saunders et al., 1988) on remote cloud cover detection systems which are applicable to aver-

* Corresponding author at: Institute of Oceanography, University of Gdańsk, al. Marszałka Piłsudskiego 46, 81—378, Gdynia, Poland.
E-mail address: marcin.paszkuta@ug.edu.pl (M. Paszkuta).
Peer review under the responsibility of the Institute of Oceanology of the Polish Academy of Sciences.

Production and hosting by Elsevier

https://doi.org/10.1016/j.oceano.2021.12.005

Figure 1 An example of cloudiness estimation and the resultant statistical error (Baltic Sea, 18 May 2017, 5:30 UTC) (LW, left-hand side; SW, right-hand side) [source: www.satbaltic.pl].

aged global-scale situations, but their actual regional-scale utility is frequently debated. Due to the nature of radiation, measuring it involves a lot of uncertainties. Cloud detection systems based on satellite data mostly use physical parameters calculated from the radiation spectrum, i.e. colour, shape, thickness, gradient, height, and inter-band relationships or interactions between the detected objects themselves (Mahajan et al., 2020). Different detection techniques as well as different classification methods are used, e.g. binary classification and measurement of cloud cover opacity based on pixel values. For the Baltic Sea region, a review of cloudiness in reference to climate change was carried out by Post et al. (2020). The study analysed the regional mean time series and regional maps of trends in the Baltic Sea area. The cloud parameters studied were total fractional cloud cover and cloud-top height. In the study carried out by Reuter et al. (2014), a SEVIRI-based cloud detection algorithm was developed for the Baltic Sea catchment area. The total cloudiness obtained from the satellite data was 0.65 compared to 0.63 for the model. Large discrepancies were observed in the 24-hour cloud-cycle phase. There was no significant trend in the total cloud amount, either from the model or from the satellite data. Li et at. (2020) proposed a cloud detection method based on genetic reinforcement learning in order to improve cloud detection at a regional scale. Banks et al. (2015) showed that the standard cloud mask used routinely in processing global ocean colour data from National Aeronautics and Space Administration (NASA) can mask optical phenomena such as intense algal blooms in the Baltic Sea. These blooms have a significant impact on the environment and require appropriate monitoring. Their findings show that replacing the standard cloud mask can increase the data accuracy by 22% during the seasonal cycle in the Baltic Sea. On the other hand, Kowalewska-Kalkowska et al. (2019) showed the difficulties and limitations of poor cloud masking over the Baltic Sea in identifying and modelling coastal upwelling. It was also demonstrated that the usefulness of this factor for predicting threats associated with extreme conditions is still limited as a consequence of the regional estimation of hazardous weather events (Latos et al., 2021). Jakobson et al. (2014) showed that the diurnal variability of precipitable water over the Baltic Sea is the inverse of water vapour variability over land. Finally, Mahajan et al. (2020) discussed the current trends and direction of development for modern regional cloud detection systems based on satellite data. A hybrid approach using machine learning, physical parameter acquisition and ground-based validation was recommended for model improvement. The cited publications mostly concern issues of improving the quality and daily variability of the data at the regional scale, which suggests that the actual usefulness of cloud algorithms is questionable. This study discusses the possibility of using a simple algorithm to assess cloudiness in regions with similar geographical conditions as the Baltic Sea. Paszkuta et al. (2019) explained those methods in more detailed recommendations. They show new results on the extent and size of cloud cover during the day and night time. Detection methods have been identified as the main source of uncertainty. First, to minimise errors, efforts were made to limit the research area to a more homogenous region. The proximity of the northern part of the Baltic Sea to

Table 1 Spectral characteristics of the SEVIRI radiometer channels.

Waveband		Spectral range (μm)			Remarks
		λ_{cen}	λ_{min}	λ_{max}	
1	VIS0.6	0.64	0.56	0.71	Atmospheric visible window
2	VIS0.8	0.81	0.74	0.88	Atmospheric visible window
3	NIR1.6	1.64	1.50	1.78	Near infrared atmospheric window
4	IR3.9	3.90	3.48	4.36	Atmospheric thermal window
5	WV6.2	6.25	5.35	7.15	Water vapour absorption
6	WV7.3	7.35	6.85	7.85	Water vapour absorption
7	IR8.7	8.70	8.30	9.10	Atmospheric thermal window
8	IR9.7	9.66	9.38	9.94	Ozone absorption
9	IR10.8	10.80	9.80	11.80	Atmospheric thermal window
10	IR12.0	12.00	11.00	13.00	Atmospheric thermal window
11	IR13.4	13.40	12.40	14.40	Carbon dioxide absorption
12	HRV	0.75	0.40	1.10	Atmospheric visible window + water vapour absorption

the northern polar circle rules out, for a considerable period of time, the possibility of using the entire bandwidth range, particularly the bandwidths in the short-wave part, and poses a serious challenge for geostationary satellites, e.g. the Meteosat Second Generation (MSG) (Bennouna et al., 2010). It is, therefore, interesting to begin with cloudiness detection broken down into shortwave and longwave band ranges, the division being important not only for the transition from daytime to night-time, but also for the measurement site. The changes will then depend primarily on the available information; for obvious reasons (including the high solar angle limitation), only data from the longwave band can be used during the night (Table 1). Differences between night-time and daytime cloud cover estimates are quite natural and are visible when comparing information from shortwave and longwave band daytime routines. The differences are explained by the physical parameters of cloudiness because high-reflectance warm formations are usually the only reference for brightness temperature studies, and cold fog does not always affect the visible radiation range (Jakobson et al., 2014; Jedlovec, 2009; Krężel and Paszkuta, 2011; Paszkuta et al., 2019). As the problem is the regional scale, different methodologies, which are a fairly important source of uncertainty, introduce artefacts emerging along the shoreline or at the edge of low clouds. The artefacts result from an incorrect estimation, e.g. with the use of the textural image analysis techniques. At the same time, they are difficult to eliminate due to convections forming in the area and the presence of near-shore effects such as upwellings. There are numerous examples of instantaneous, regional over- and underestimation of cloudiness in the atmosphere. Figure 1 shows examples of differences in cloudiness estimation done by operational detection systems during the day and night. The date and time (Figure 1) was chosen due to the apparent variability of data and the availability of a wide range of different types of cloud cover. Generally, methods adapted to the global scales (Figure 2), show the daytime cloudiness to be lower when compared to regional scales (Figure 1), with the night-time cloudiness being comparably higher. For this reason, the averaged characteristics show relatively small differences which increase with the change of the Solar Zenith Angle (SZA): the higher north, the larger the difference due to a change in the proportions between the daytime vs. night-time routines. In many comparisons, it is difficult to unequivocally state whether and which physical process is responsible for the differences between the routines. It is certain, however, that the presence of a large body of water substantially affects the detection results, and physical analyses should be conducted separately for the daytime and night-time routines. The paper is an extension of the study conducted by Paszkuta et al. (2019), but it is the first study to show the optimisation of the algorithm in the process of generalizing Planck's law based on satellite results and published materials. To reveal the variability in the detection of diurnal Baltic Sea cloudiness, the results are compared with alternative sources and the North Atlantic Oscillation (NAO) index. The goal is to increase the quality of oceanographic data. An overestimation of cloudiness can often deprive us of information about important sea surface phenomena that can last several hours, such as coastal upwelling. An underestimation can have a negative impact, e.g. on the balance of radiation reaching the sea surface. The aim is to identify and estimate the source of uncertainty arising from the satellite measurement process. Clearly, considering the availability, scope and amount of information, satellite measurements have an undeniable value. The article consists of five sections. In Section 1 the problem is described using the example of the briefly summarised SatBaltic project, the state of knowledge on cloud detection using satellite data is presented, and daily analyses taking into account some outside factors on the Baltic are performed, followed by a literature review. Section 2 focuses on the description of data used in the analyses and suitable for comparing the differences between day and night values. The methods used in the paper are based on the technique published and presented in detail for the first time by the authors, which consists in linearising Planck's law. It has been proposed to improve the method further. In Section 3, we clearly describe the modifications to that method and the changes in cloud cover detection. In Section 4, we present

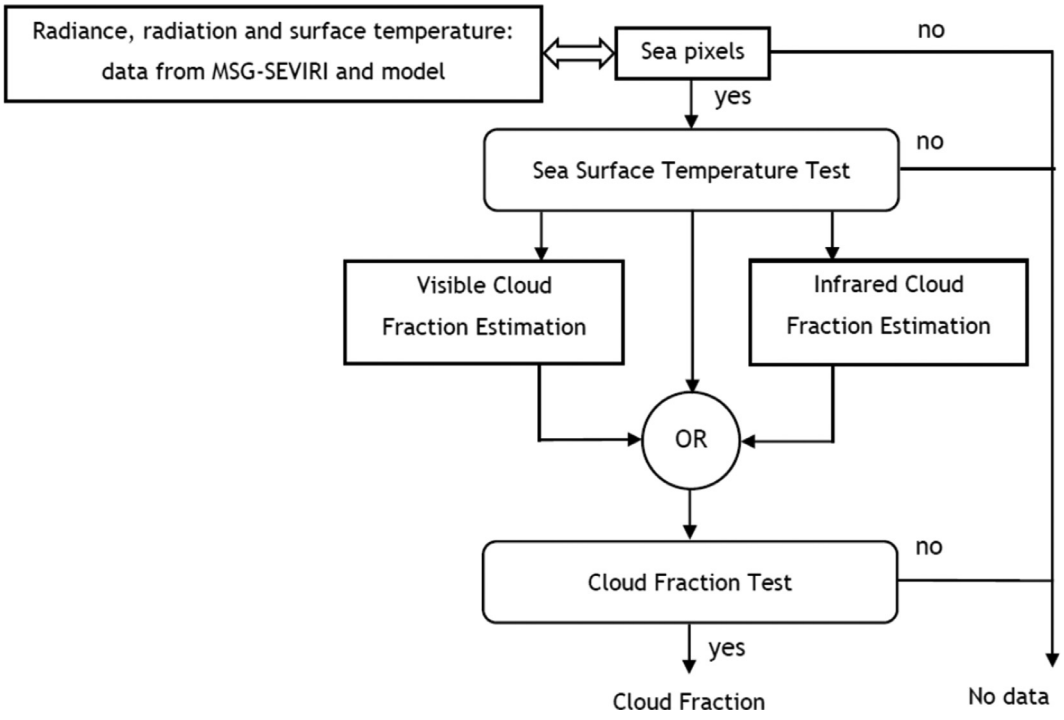

Figure 2 Block diagram of the cloud detection data flow (Paszkuta et al., 2019).

the significance of our findings. In the last section, we discuss the results and list the probable reasons for the differences.

2. Material and methods

A flagship product of satellite cloudiness data developed within the SatBaltic project (Woźniak et al., 2011a,b), consists of a series of tests using the split-windows technique and model estimations for cloudless atmosphere (Figure 2). The detection technique is, in principle, based on a difference between the Spinning Enhanced Visible and Infrared Imager (SEVIRI) ranges (Table 1) and compares the outcomes with values modelled for cloudless conditions. It generalises radiation transmission equations using relationships between two neighbouring spectral bands, and is, in fact, based on the magnitude of the difference between them (Kriebel et al., 2003; Kryvobok et al., 2005). The technique of split windows and model estimation for the cloudless atmosphere at the Baltic Sea was used both in the short and long range of waves. In this way, the SatBaltic system uses two values of the cloud fraction: one referring to shortwave radiation and the other to longwave band. The difference between the magnitude of radiation at full cloudiness and in the absence of clouds under identical thermal conditions over the Baltic Sea may be as high as 120 W m^{-2}. The semi-empirical formulae reported in the literature are frequently based on the general cloudiness function as the main factor determining the bottom-up flux of longwave-band radiation. This is, however, a far-flung approximation which may be subject to a statistical error of as much as even 30% (Zapadka et al., 2015). The characteristic feature of the method proposed is that it is region-specific and based on radiation models developed by the authors to avoid relying on external sources. Similarly to most of the studies referred to, the division into daytime and nighttime is included, with the incident radiation angle of 67° being used as a criterion (Paszkuta et al., 2019). The differences in the diurnal cycle of cloud cover, and hence in the radiative cycle, can lead to significant changes in the energy balance. Clouds generally attenuate the solar radiative energy flux. The problem of absorption or transmission by different types of clouds has been explained in the literature (Kaczmarek and Dera, 1998; Rozwadowska, 2004). The Baltic Sea has thermodynamic properties that are different from those of the land and the oceans, and some of those properties have a significant influence on the atmosphere. Seawater is subject to constant phase changes that absorb large amounts of energy. The energy required for these processes comes mainly from the atmosphere. Therefore, changes in the water can cause significant changes in the atmosphere, which occur in a continuous diurnal cycle, different (on a different scale) than in the open oceans. The air temperature varies by a few to a dozen degrees per day, with little change in water temperature. Therefore, it happens that the water in the Baltic Sea has a higher temperature than the air as a consequence of air temperature fluctuations. If the sea is cooler than the air, the water will draw heat from its surroundings in an attempt to compensate for this difference. Conversely, when the water in the sea contains more energy, the air temperature changes. These mechanisms can partly explain the diurnal differences in cloud cover. At night, when the air warms up, it rises higher. When the rising air reaches the height where condensation occurs, the conditions for the formation of clouds occur. During the day, the situation can reverse and a cloud-free atmosphere can form. If the water is warmer

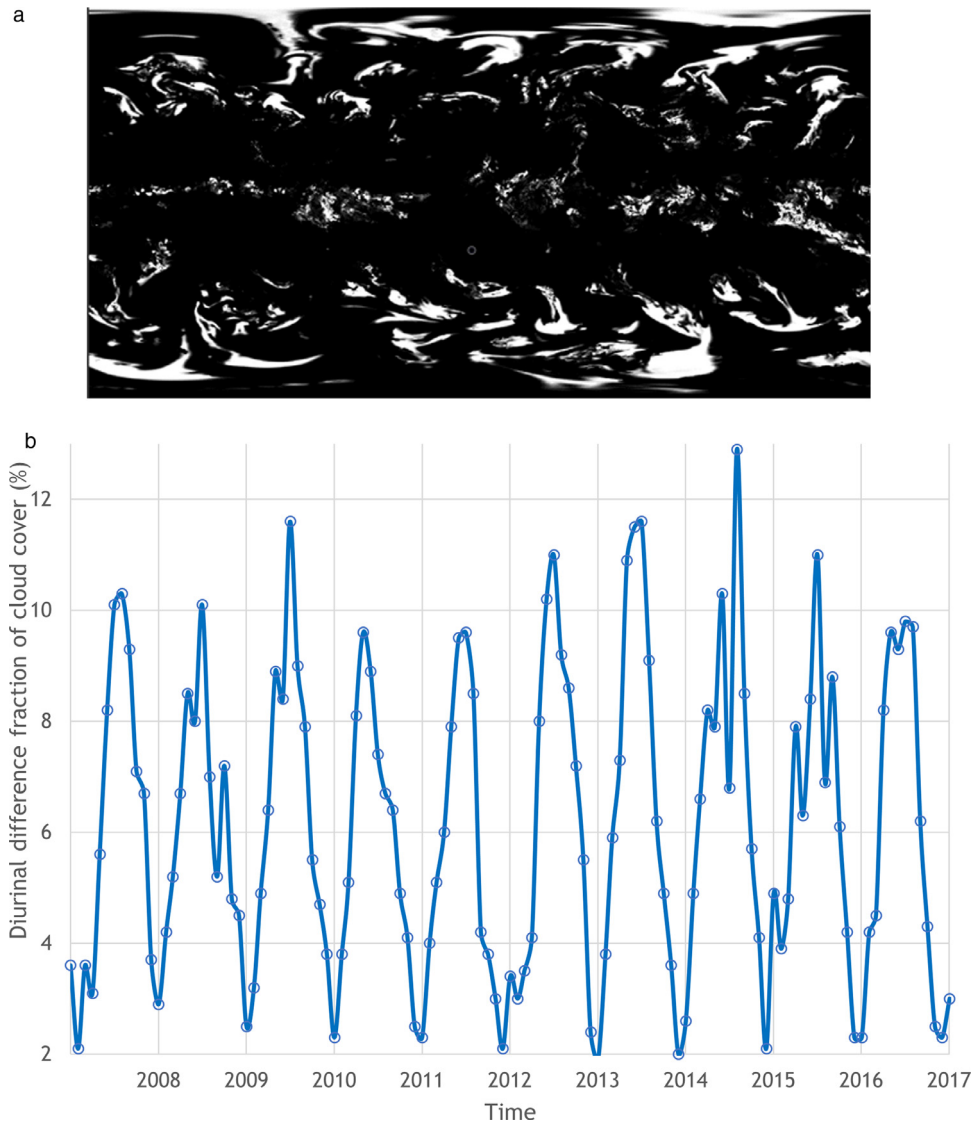

Figure 3 Example of global fraction of cloud cover on 5 May 2017 at 12:00 UTC (a), and (b) Monthly average diurnal variation fraction of cloud cover for the Baltic Sea, data obtained from ECMWF—ERA5 (https://cds.climate.copernicus.eu).

than the environment, clouds may even form around the clock. Based on the European Centre for Medium-Range Weather Forecasts climate reanalysis data[1] (ECMWF—ERA5) shown in (Figure 3), the average daily difference in the percentage of cloud cover on the Baltic Sea (between 2008 and 2017) was up to a few percent, depending on the location and season: a maximum of 13% was recorded which is lower than the value obtained in the study using satellite data. This confirms the results obtained by the authors; however, the question remains whether these phenomena have natural causes. The daily changes in cloud cover over the Baltic Sea shown in the study could even modify the atmospheric circulation, if they have a natural basis. In the rest of the paper, we will identify other causes that are not indicative of natural physical processes. It is interesting to look for trends and long-term changes in the climate related to the cloud cover parameter; however, at the moment, this is not the subject of this analysis, although the arbitrary period of 30 years of climate changes already covers the period of data collected by satellite instruments. The satellite-based cloudiness data calculated by the Advanced Very High Resolution Radiometer (AVHRR) (mounted on the Tiros N satellite series operated by the National Oceanic and Atmospheric Administration, NOAA) is based on the AVHRR Processing Over Land cLoud and Ocean (APOLLO) algorithm (Saunders and Kriebel, 1988). The algorithm involves five independent tests. It analyses a sequence of threshold, textural, and inter-waveband relations. Significantly, one of the routines is dedicated to marine areas and simultaneously analyses the relationship between short and longwave channels while using separate series of daytime and nighttime data (Cracknell, 1997). Results of the algorithm have been repeatedly compared with alternative solutions and in situ measurements (Kriebel et al., 1989). The AVHRR data, owing to the regional measurement system, does not have an inferior spatial structure to the data generated by SE-

[1] https://cds.climate.copernicus.eu

VIRI. From the standpoint of instantaneous regional observations, the MSG is more advantageous for the measurement of rapidly changing cloud cover (particularly at the estimated range). Average differences between the data generated by AVHRR and SEVIRI are up to several per cent, the values being higher for the night-time data. The cloud products offered on-line from MODIS data combine the IR and VIS ranges, similarly to the algorithm proposed in this study. The cloud fractional cover product developed in 2004 by the Satellite Application Facility on Climate Monitoring (CM SAF) consortium within the CLoud property dAtAset (CLAAS-2) using SEVIRI (Edition 2) (today the Interim Climate Data Record [ICDR]) is based on NWC SAF cloudiness detection and classification algorithms. The Cloud-Aerosol Lidar and Infrared Pathfinder (CALIPSO) was designed to investigate the effects of clouds on the radiation budget (Chepfer et al., 2013). Equipped with the Cloud-Aerosol Lidar with Orthogonal Polarization (CALIOP), the device offers information based on active detection.

3. Results

3.1. New approaches

In line with the goal of this study, we estimated the averages for daytime and night-time events separately. According to this important classification, the data sets relate to physical processes taking place during the day and at night. Although marked differences in cloudiness between the day and the night, such as those discussed in the previous section, are likely not to have physical underpinnings, certain differences in the emission of the sea will always happen. They emerge, for example, due to the cyclical course of solar radiation and its consequences during the daytime, whereas at night they occur because of, e.g., the formation of a humid zone just above the sea surface, which affects the long waveband emission. For the IR range, the method is based on the three-dimensional numerical hydrodynamic M3D model (Kowalewski, 1997), which allows us to calculate the emission temperature of the sea both during the daytime and at night. As the T_9 (9.80—11.80 μm) and T_{10} (11.00—13.00 μm) frequency bands are close on the spectrum (Table 1), the first approximation disregarded the non-linear nature of Planck's law, and brightness temperatures in the SEVIRI channels were estimated from the modelled sea-surface temperature (*SST*). This simplification (approach 1) has some advantages, as it produces more general results, but involves unavoidable errors which, owing to the structure of the algorithm (the difference between the two wavebands is estimated with comparable uncertainty) may only be acceptable on account of the broad objectives of the detection model. The relationships can be illustrated as:

$$T^M = SST_{M3D} \cdot A, \tag{1}$$

where T^M equals estimated brightness temperature; SST_{M3D} equals sea surface temperature determined by M3D; A equals calibration constant from Table 2.

This approximation assumes the coefficient which in fact causes the ratio between the black body and true emission in the SEVIRI channels 9 and 10 to approach one. The coefficient should be understood as an effect of averaging the daytime and night-time values calculated according to the split-window formula and simultaneously taking into account the differences between the surface temperature and the *SST*. More detailed estimations based on the IR range for the day and the night should result from different emissive characteristics of the spectral bands used. The problem seems to be well-explored for the sea surface; unfortunately, the emissivity of inhomogeneous cloud layers at poor radiation is difficult to measure. This is one of the reasons why noticeable differences, resulting from the nature of the radiation itself, occur when the cloudiness coefficient is calculated from VIS and IR. Should the emissivity values (a coefficient showing the difference between the properties of the true body and the black body) be switched, the radiation in the channel would — depending on the temperature — be higher or lower at the same values of the emitting body temperature. In the first approximation (approximation 1 in Figure 7), the relationship was a priori assumed to be linear, which influences the difference between the daytime and night-time cloud cover detection. To solve the problem of the non-linearity of Planck's law, the subsequent approximations 2 and 3 use two different radiation transmission equations, one for the night and the other for the day for the same thermal channels. The function of fitting the spectral radiation to the black body radiation is non-linear (Figure 4) and makes it possible to, e.g. measure *SST* using satellite techniques (Wang et al., 2019). Radiation emitted by the sea surface in the range of IR wavelengths recorded by SEVIRI can be approximated by a function correlating

Table 2 Estimation constants for the SEVIRI thermal channels.

Channel	*k*	*A*	*B*	*C*
$T^M{}_9$	9.3066	0.992	0.627	0.9983
$T^M{}_{10}$	8.3966	0.998	0.397	0.9988

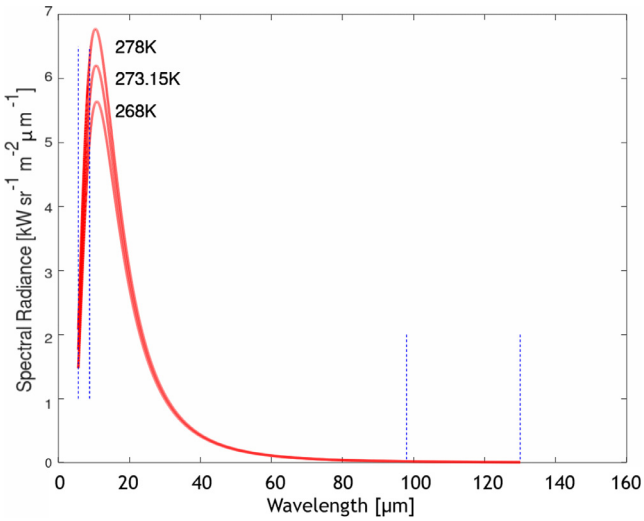

Figure 4 Planck's law for the temperatures analysed, with spectral ranges.

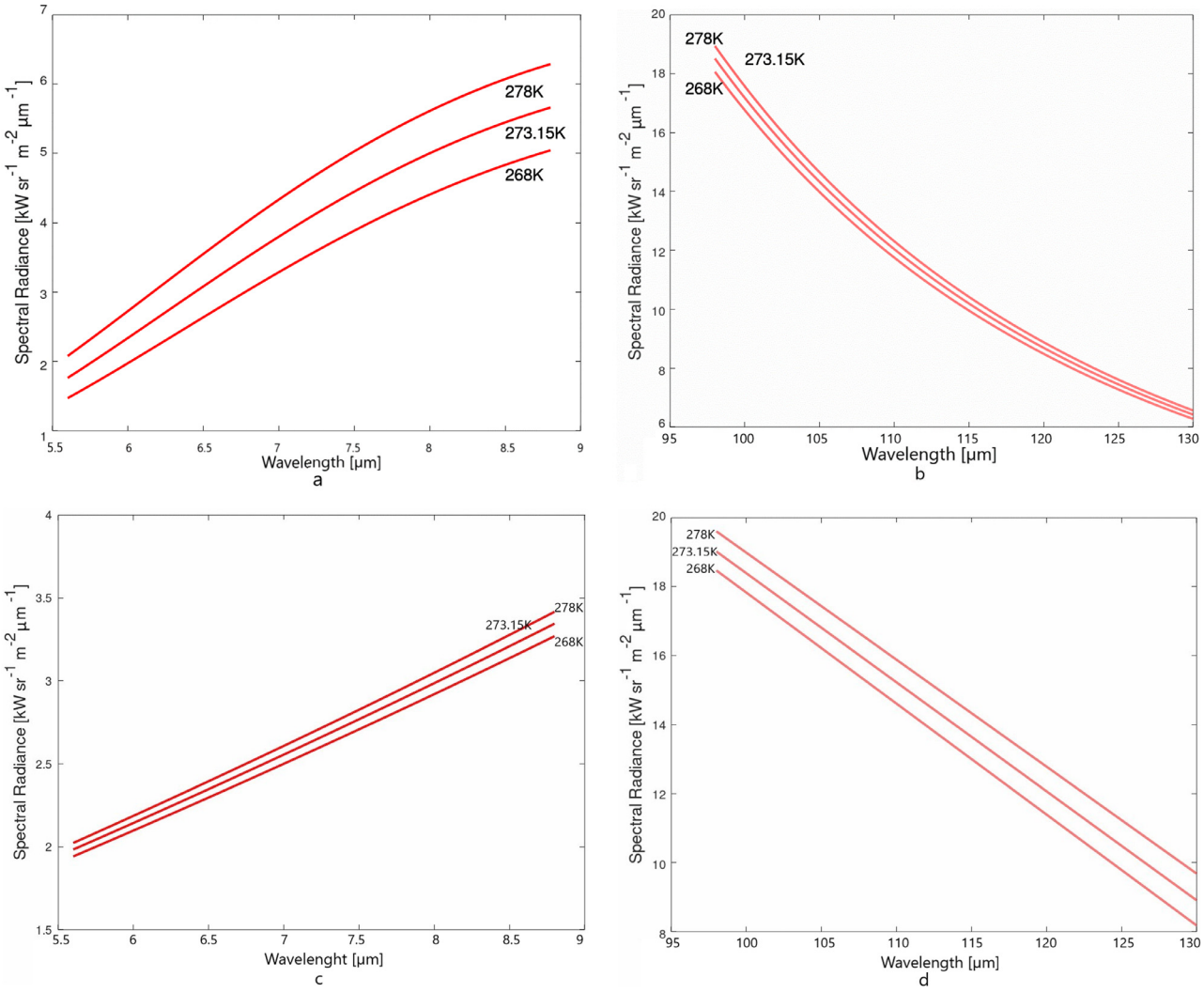

Figure 5 Examples of linear approximation of Planck's laws to: a,c) Short; b,d) Long; wave-areas analysed in the study.

with the Planck function:

$$I(\lambda) = \varepsilon F \frac{2hc^2}{\lambda^5} \frac{1}{e^{hc/\lambda k_B T}}; \qquad \left(\frac{hc}{\lambda k_B T} \gg 1\right), \tag{2}$$

where: ε equals ambient emissivity; F equals device-specific coefficient involving geometric and radiometric factors; T equals black body temperature; λ equals wavelength; h equals the Planck constant; c equals light speed; and k_B equals the Boltzmann constant.

Eq. (2) is valid provided that $hc/\lambda kT >> 1$, i.e. the wavelength is below the function maximum. Figure 4 and Figure 5 show blackbody radiation in the detection temperature range for semi-transparent objects, i.e. objects with radiation emission similar to that at sea. Spectral ranges corresponding to the channels analysed in this work are marked. As the temperature increases, the function maximum (the near-IR) shifts towards shorter wavelengths. This behaviour is described by the Wien's law, $\lambda = b/T$, where b equals 2.8978 $\times$ 10^6 nm-K. As seen in Figure 4 and Figure 5, the spectral ranges marked are below the function maximum. This presents a challenge for satellite-aided remote sensing, because it means that the intensity of the signal analysed will be correspondingly lower. In such cases, when the brightness temperature of the atmosphere is close to that of the sea surface, certain linearisation of Planck's law is observable (Figure 5). An appropriate transformation of the function simplifies it to $1/\lambda$:

$$\ln(\lambda^5 I) = \ln\left(2hc^2 \varepsilon F\right) - \frac{hc}{k_B T} \frac{1}{\lambda}. \tag{3}$$

This makes it possible to carry out linear fitting to the linearised radiation spectra. In addition to advantages related to usability, this operation ensures an ideal representation of deviations by the blackbody curves. Therefore, the fitting can be carried out in a more universal form, excluding naturally non-analysed parts of the non-linear spectrum. This is particularly useful at temperatures corresponding to shorter wavelengths where uncertainties are crucial and the blackbody radiation is relatively low. Non-linear procedures call for the fitting of the Planck formula parameters (ε, F, T, and λ) which are less sensitive than those of the linear equation and, if they are different from true values, the fitting will not converge (Wang et al., 2019). The brightness temperature computed on the basis of satellite sources is based

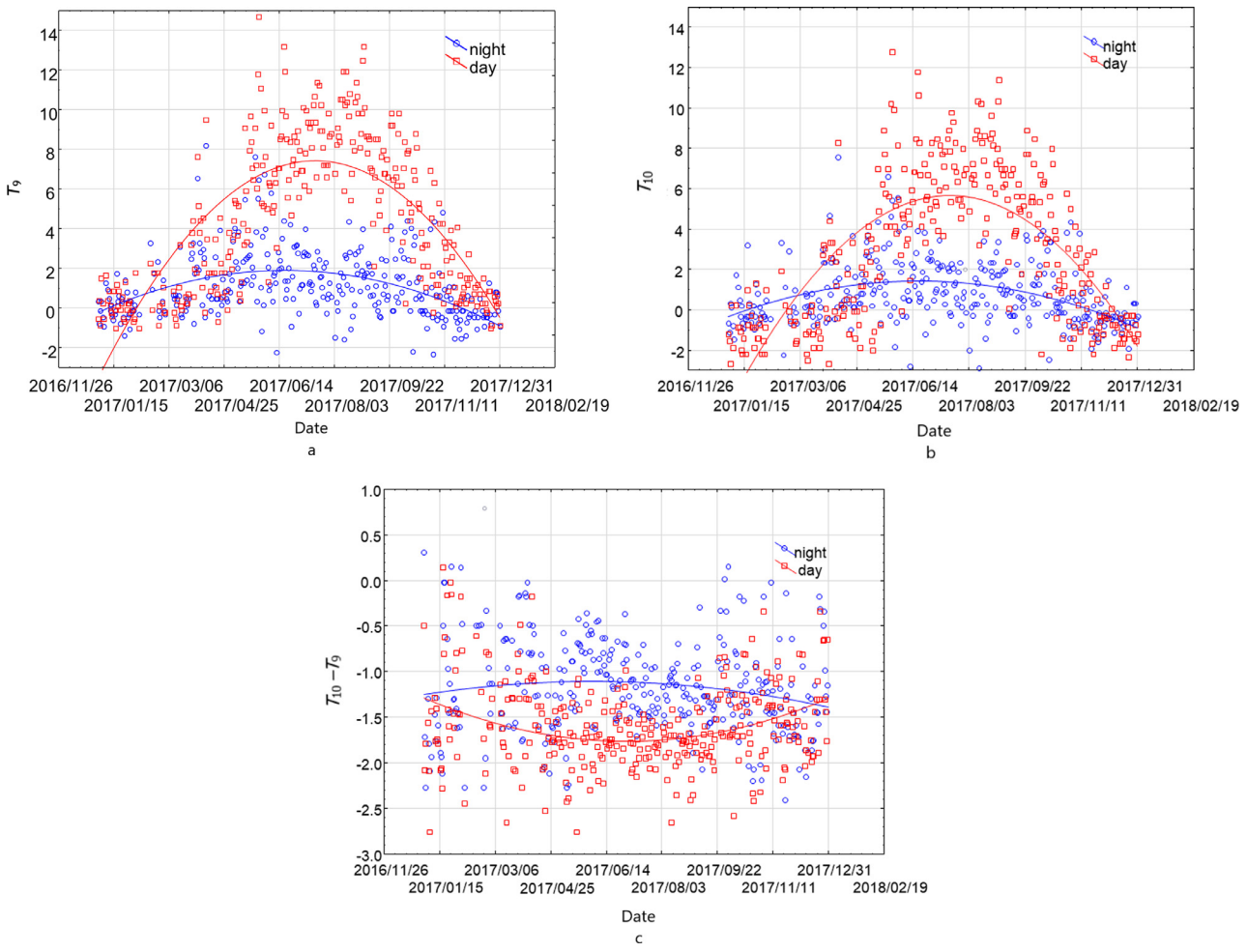

Figure 6 A comparison of daytime and night-time MSG data series cloudless sea in 2017: a) Radiation temperatures in channel 9; b) Radiation temperatures in channel 10; c) Difference between the (10—9) radiation temperatures for the BalticBeta station. Filled shapes for May 17.

on Planck's law, but *SST* (determined by the M3D), used to calculate the brightness temperature under cloudless conditions, not necessarily does. The temperature ratio proposed in this study includes the *SST* with an identical value within channels 9 and 10, multiplied by the linear factor. Unfortunately, in reality, brightness temperatures differ across different spectral ranges, although the difference may be small. Generally, the source of temperature may be of no importance if multiplied by the fourth root of the emissivity coefficient. In an appropriate channel, the result is the emission temperature in this spectral channel. According to the Stefan—Boltzmann law, the amount of thermal radiation estimated for a satellite channel from brightness temperature is:

$$\begin{aligned} L &= \varepsilon\sigma SST_{M3D}^4 \\ L &= T^4 \\ L &= (\varepsilon)^{\frac{1}{4}}\ SST_{M3D}. \end{aligned} \tag{4}$$

According to Masuda et al. (1988), at the wavelength of 10.8 μm (SEVIRI channel 9) and at the latitude of the Baltic Sea (SZA of about 60°), emissivity is about 0.967. Obviously, the emissivity determined this way will additionally depend on the SZA and wind speed; including these factors will produce the constant A as shown in Table 2. The coefficients calculated are the fourth roots of the emissivity coefficient. Figure 7 provides a comparison between results obtained with the algorithm proposed earlier, broken down into successive approach 1 with Eq. (1), approach 2 with Eq. (3) and approach 3 with Eq. (4). With such approaches, however, the daytime and night-time data are difficult to compare because the situations are completely different. This will be important for the identification of the common parameter which affects, e.g. the value of transmission or emission. Within 24 hours, the temperature of both the clouds and the atmosphere can vary significantly. In the algorithm, *SST* is of only auxiliary importance. It will never be ideal, because it stems from theoretical estimation. Therefore, emissivity was determined empirically, that is, cloudless events were selected — in a controlled manner — for pixels T_9 and T_{10}. Figure 6 shows the relationships (for 2017) between brightness temperatures measured at 12:00 and 00:00 UTC in channels 9 and 10 and the differences between them. Calculations were made for areas identified as cloudless, conditionally and simultaneously at 12:00 and 00:00 UTC.

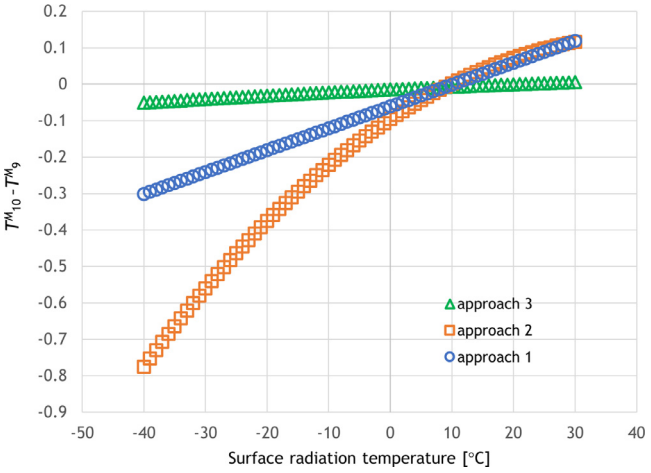

Figure 7 Evolution of the IR cloudiness algorithm: a modelled difference between satellite channels as a function of the surface radiation temperature.

Figure 6 allows us to conclude that during the day the sea warms up in synchrony with the solar zenith angle (in summer and spring the most) and tends to cool down during the night. The previously mentioned example of May 17 (Figure 1) was marked with filled shapes. It is not the cooling-down itself that is interesting, but its extent. Statistically, the cooling-down effect is included in radiation budgets; unfortunately, however, it cannot be observed in radiation models, e.g. in the M3D. To demonstrate the changes in the physical properties of the water during the night, an additional analysis of the $T_{10}-T_9$ difference was included in Figure 6c. This way, we learned that physical properties of the water do undergo diel changes. This confirms the hypothesis that, if cloudiness is derived from IR channels, different methods ought to be used for the night and for the day. Interpretation of the effect during the daytime in the VIS range is undoubtedly related to absorption and to evaporation at night. The general formulae showed in the functional diagram (approximation 1, Figure 7) should be modified to better fit the regional conditions by means of non-linear combination of the Planck function and the spectral wave length (approach 2 and approach 3, Figure 7). It is assumed that the relationship between radiation in two neighbouring spectral bands is non-linear, whereby the diel period should be divided into at least two zones: the daily and nightly zone:

$$T^M = \frac{c_1 k}{\left(\ln\left(\frac{c_2 k^3}{SST_{M3D}} + 1\right) - \mathrm{B}\right)\mathrm{C}}, \tag{5}$$

where T^M equals brightness temperature [K], k equals wave number [m^{-1}]; c_1=0.014388 K m, and c_2=119.10659 mW sr^{-1} m^{-7} are empirical constants; while the remaining values are the same as defined in Table 2 (EUMETSAT, 2007; EUMETSAT, 2012). In the last approximation, for a more effective illustration of the difference between the day and the night, we applied Planck's radiation law directly. This time, we used the calibration values of the satellite radiometer as measured prior to launching. The brightness temperature can be estimated as:

$$T^M = a_0 + a_1 T_S + a_2 T_S^2, \tag{6}$$

where:

$$T_s = \frac{ch}{\kappa\lambda(ln(\frac{2c^2h}{\lambda^5 SST_{M3D}} + 1) - B)C},$$

a_0, a_1 and a_2 are constants fitted to every SEVIRI band, available from the European Space Agency catalogue.

Like earlier, the SST_{M3D} is calculated for each pixel by the M3D. The remaining constants are defined in Table 2. The development of the cloudiness algorithm from long wavelength channels in Table 1 generally involved a technical fitting of the formula to the constraints of the satellite device. This should restrict the uncertainties generated by the first approximation. The solutions proposed treat the cloudiness data (for brightness temperatures >-3°C) and clear sea in a characteristic manner. The second Eq. (3) and third Eq. (4) approximations involve the non-linear Planck's law (Figure 7). The difference between the channels is most pronounced in the second approximation: while considering channels with the ability of remarkable cloud detection, the differences are in agreement with the first approximation Eq. (1), and the differences for temperatures corresponding to cloudy pixels are considerable. The general underestimation and overestimation of satellite cloud detection was analysed taking into account the full available channel range. In the analysis, they were taken into account according to the detection algorithm. However, there is a high risk for cloud cover to be overestimated and for clear pixels to be classified as cloudy. Approximation 3, Eq. (4), produced a completely different pattern. While retaining non-linearity, it poorly reflected the difference. Results of comparing the approximations shown in Figure 7 along with estimations from short wavelength channels proposed below are discussed in the next section. As the cloudiness (extent and type of clouds) changes, the magnitude of the satellite signal recorded alters as well. As demonstrated above, this also affects the change in the VIS radiation difference between the neighbouring satellite channels. Under cloudless conditions, the difference remains more or less stable. The values can be estimated from a radiation model, e.g. the Solrad model (Krężel and Paszkuta, 2011; Krężel et al., 2008). Such operations require estimation of the radiation from the Earth surface to the satellite radiometer.

3.2. Comparison of calculated and estimated equivalents of cloud cover

The methods described above were used to determine the unitless equivalent of cloudiness, an equivalent of the 'cloud fraction' calculated from external sources due to different terminology used in the literature to define the same cloudiness variable for the marine environment. The validation involved both qualitative and quantitative aspects. Estimations were performed for instantaneous and temporary averaged situations. The qualitative analysis of the cloudiness product involved a comparison between irradiance data series recorded in 2017 by stationary instruments at Lotos Baltic Beta stations (55°28′50.67″N, 18°10′54.03″E) (data from the SatBaltic portal). Information on the empirical data used is detailed in the publication by Zapadka et al. (2020). The comparison of in situ data with cloudiness val-

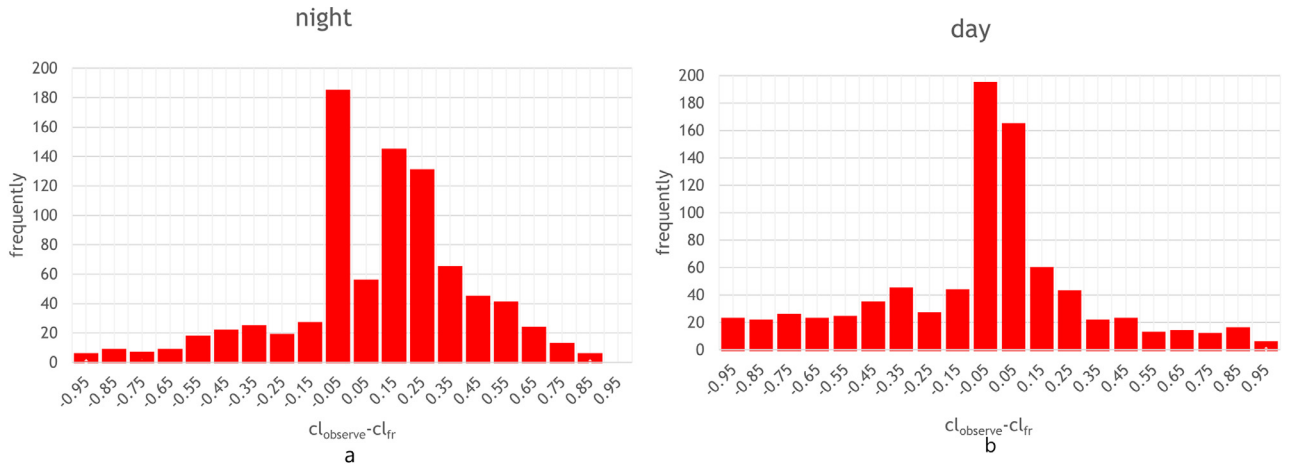

Figure 8 Distribution of the differences between the cloudiness estimated in situ and calculated from satellite data: a) at night (data collected during the day was applied to the night-time algorithm); b) during the day; the data was collected on 26 April 2019 on board of the r/v *Oceanograf*.

ues estimated from the satellite-derived data requires generalisation of reference points assigned not only to the place, but also to the time of the nearest available projection. This pertains to both VIS and IR routines. Therefore, most of similar analyses show fairly large uncertainties associated primarily with the methodology of the measurement itself, and use radiation information collected during the day. At this stage, estimation showed about 80% of the cases to be estimated correctly, which means that in 20% of the cases the algorithm may be 100% wrong: cloudless areas may be interpreted as completely clouded (in IR situations) and vice versa.

Figure 8 shows the distribution of differences between the cloudiness equivalent estimated on land ($cl_{observe}$) and calculated from satellite data for the night (clfrIR, Figure 8a) and the day (clfrVIS, Figure 8b). The largest discrepancies occur when the value of a pixel is estimated by averaging a totally cloudless and clouded area. The former situation may be rectified by appropriately testing the channels, while the latter may be corrected by applying appropriate validation techniques and procedures. The remaining differences are most likely caused by the detection methodology. Figure 8 shows exclusively the daytime data series, i.e. for SZA less than 67°, the cloudiness was estimated with the night-time algorithm for measurements taken during the day (in the long waveband channels only). Calculations for the night-time scenario in Figure 8b, conducted with an algorithm published by Paszkuta et al. (2019) showed the mean of 0.06, standard deviation of 0.34, and the correlation coefficient of 0.66. Figure 8a illustrates the distribution of the differences between the cloud cover estimated with the daytime routine (in the shortwave-band channels); while deviations that appear due to the precision of waveband range were calculated from the solar constant and the Solrad results for cloudless atmosphere. The difference between the estimated cloudiness for the daytime routine showed the mean error of 0.12, standard deviation of 0.26, and the correlation coefficient of 0.77. In order to restrict the error of measurement, our further analysis involved routines that show the best characteristics, with the methodological error reduced to the minimum under the current conditions. The quantitative characteristics were applied for the entire 2017 for data acquired with different detection systems and satellite devices.

4. Discussion

The cloud factor (Paszkuta et al., 2019) was averaged temporally and compared with the unitless cloudiness parameter (tentatively termed the 'cloudiness equivalent' because of the need to standardise the results within 0—100%) produced by various satellite systems available on line: APOLLO (The Cloud Physical Properties Royal Netherlands Meteorological Institute) (Kriebel et al., 2003), CM SAF (The Satellite Application Facility on Climate Monitoring) (Finkensieper et al., 2018), MODISCP (The Moderate Resolution Imaging Spectroradiometer Cloud Product) (Platnick et al., 2017) and CALIPSO—CALIOP (Cloud-Aerosol Lidar Pathfinder Satellite Observations—Cloud-Aerosol Lidar with Orthogonal Polarization) (Chepfer et al., 2008; Winker et al., 2009). It should be mentioned that these systems compute data separately for the shortwave and longwave bands, using different satellite sources, thus rendering the analysis still more valuable. Figure 9 illustrates the relationship between cloudiness (termed differently and variously standardised in different systems, hence the general term 'equivalent') that has been normalised for the needs of this study to the common conversion factor in the range of 0—100%. Despite substantial differences in instantaneous estimations, the routines show the mean annual cloudiness over the Baltic Sea to be at a similar level of about 64%. As could be expected, the highest and the lowest cloudiness was recorded during winter (November—January) and summer (May—August), respectively. This trend was repeated by all the systems. At the monthly averaging level, substantial differences in the amount of cloudiness, of up to several per cent, can be seen. The increase in the difference between the systems in cloudiness estimations may be associated with the true magnitude of cloudiness which is at its lowest in summer (3—4%) and may be as high as several per cent in winter. Because data from all seasons was used, the

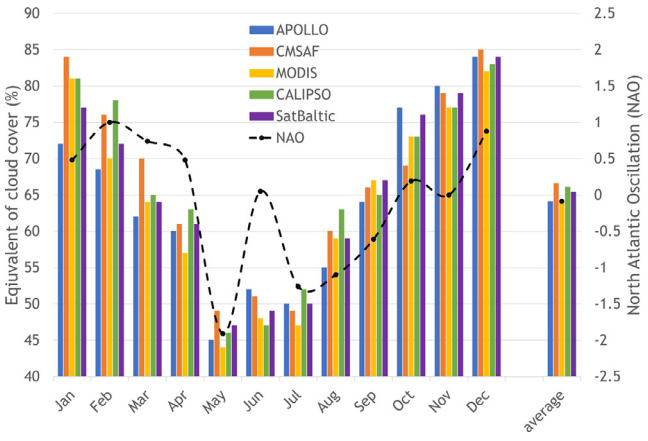

Figure 9 Different estimates of average monthly equivalent of cloud cover (colour-coded), and the NAO index (dashed line) for the Baltic Sea basin in 2017.

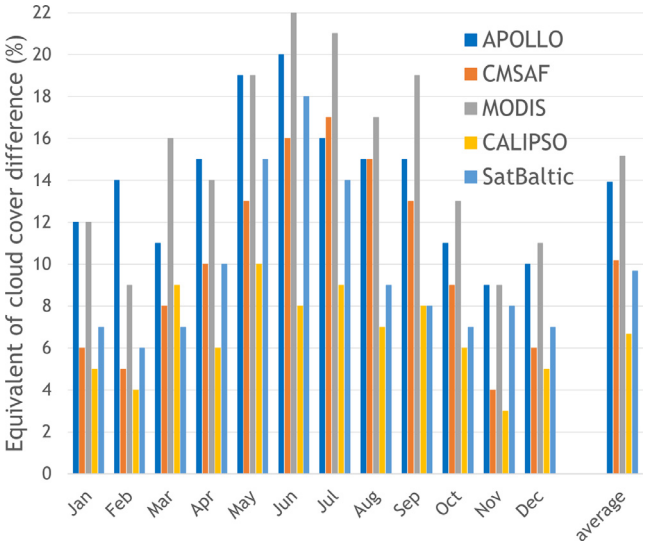

Figure 10 The absolute difference between the cloudiness equivalent determined during the day and at night (%).

impact of meteorological parameters may be significant. In Figure 9, the general weather property is represented by the NAO (North Atlantic Oscillation) index (Jędrasik and Kowalewski, 2019) as a function of cloudiness. The quantitative dependence of variables is represented by the dashed line. The NAO oscillates in the positive (NAO $>$ 0) and negative (NAO $<$ 0) directions. The positive phase represents the period of the strong Azores and deep Icelandic Atmospheric Lows, which move large air masses containing heat and moisture to the area of Northern Europe (including the Baltic Sea). As a result of low movement (from the west to the east), there is an increase in cloud cover/reduction of direct upwelling radiation, the number of storms and an increase in wind speed (Jędrasik and Kowalewski, 2019). There are thaws in winter, and frequent rainfall and temperature drops in summer. During the negative phase, there are opposing conditions, as humid air masses are moved by baric systems (weaker by the Azores High and shallower by the Icelandic Lows) towards the Mediterranean Sea. Continental masses from the east and north-east flow to the area of Northern Europe, which consequently generates sunny and cloudless summers and severe winters with reduced cloudiness. In Figure 9, the monthly trend of cloudiness in 2017 shows a decrease from January (about 80%) to May (20%), a slight increase in June and July (a little over 30%), and a regular increase from August to December (40% to 90%, respectively). Almost simultaneously, the fluctuations of the NAO index rise from the positive phase (NAO $=$ 1.6 in January) and fall to $-$2.0 in May, then alternately rise and fall to the negative phase in June and July. In the subsequent period that year, from August to December (fall–winter), the index value rose to 0.95, thus indicating a transition to the positive phase. The correlation seems to be obvious, as the decrease of cloud cover at the beginning of the year follows the decrease of the NAO index, which, during the winter, represented the conditions of intense Atlantic circulation over the Baltic Sea. Light cloudiness causes the solar radiation to increase. Slight variations (increase in June and decrease in July) in cloudiness are accompanied by an increase in the values of the (negative) NAO index. From August to December, there is a steady increase in cloudiness and a shift of the NAO index from the negative to the positive phase, characterised by a return to the Atlantic circulation.

The dominance of the positive phase in the autumn–winter period in the Baltic Sea area confirms the crucial role of the winter circulation in the NAO/North Atlantic Oscillation (Hurrel, 1995). More discussion on the conditions of the NAO index in relation to cloudiness in the Baltic Sea is presented by Gomis et al. (2008), Jędrasik (2019), Lehmann et al. (2002), Ruiz et al. (2008). Generally, data averaging increases the similarity between the methods: the longer the data series averaged, the more convergent the results. For the needs of this research, due to the nature of the measurements, it may be assumed that the lowest cloudiness deviations were obtained with measurements conducted with the active CALIPSO methods. Using this data series as a reference, the methods producing higher and lower values can be treated as over- and underestimating the measurements, respectively. Figure 10 shows the relationship between the absolute differences in cloudiness estimated during the day and at night. The differences between the methods used are fairly distinct and range from a few to several per cent. Should the differences be more or less consistent, an effect of the physical parameters of cloudiness could be suspected, but the differences suggest a methodological issue with most of the data sources, which can be rectified technically. The difference increases in summer, i.e. when the estimated cloud cover is at its lowest. The absolute difference between day and night is not mainly a function of the cloudiness: it is mainly the result of the measurement method. One may try to relate it to the day-to-night length ratio, particularly in winter for the northern areas of the Baltic Sea when darkness prevails over much of the diel cycle. As could be expected, the lowest difference was shown by the CALIPSO data series. The value of 8% is closest to the absolute day vs. night difference. Disregarding the averaging effects and lidar data modelling, it may be assumed that the differences between various systems result from the methodology of cloudiness assessment. Chepfer et al. (2019) combine satellite observations of cloud profiles and relative humidity profiles to document

diurnal variations in water vapour and vertical cloud distribution. While the average daily water vapour and cloud profiles are different over the land and the ocean, their day-to-day changes from their daily averages have similar characteristics. The relative humidity and optically thin cloud fraction profiles change together, reaching the maximum values in the troposphere at night and the minimum values during the day. It has been shown that when atmosphere over terrestrial regions shows a diurnal positive anomaly for low thin clouds, there are positive anomalies of opaque clouds in the lower atmosphere over oceanic regions in the second half of the night, which continue to grow until sunrise. According to Bergman et al. (1996), most of the diurnal variation in cloudiness is explained by regressions of only three variables: the daily solar position, the surface temperature, and the cloud level. The diurnal variability of cloudiness does not show a strong correlation with any climatological variable, as the variations are geographically independent and thus highly consistent spatially. Bergman et al. (1997), studied the diurnal variation of cloudiness over time and found that the effect of clouds on radiative fluxes is due to the diurnal variation of their properties. Time-averaged energies are obtained from radial transfer calculations in which cloud cover, temperature, and humidity are estimated from satellite observations.

5. Conclusions

Results obtained with the algorithm proposed showed the average cloudiness at night to be higher by a few per cent than during the day, the results being similar to those produced by standard routines. This difference may stem from natural or procedural causes. Therefore, regional algorithms should not rule out the natural character of the marine environment. However, results of similar satellite-based estimations should be treated with utmost caution because detection methods remain the primary source of uncertainty, which is usually explained by technical problems associated with low quality of the data. Unfortunately, there is no reliable information which would confirm that the changes over the Baltic Sea are significant enough to modify atmospheric circulation and increase/decrease the cloud amount by several per cent, which would suggest a natural cause of the changes. As the location and even the time of the uncertainty are known, it is possible to develop a targeted correction method. For this reason, application of the algorithm results to environmental studies on a regional scale should consider the factors that have a potential to improve the reliability of data. The obtained results can be successfully used to determine the average cloud cover metrics over the Baltic Sea because the analysis is inter-seasonal and climate comparisons do not show much correlation. Finally, the procedural factors responsible may be associated with radiation transmission through the atmosphere and, obviously, with the conditions of the solar radiation flux.

References

Anthis, A.I., Cracknell, A.P., 1999. Use of satellite images for fog detection (AVHRR) and forecast of fog dissipation (METEOSAT) over lowland Thessalia, Hellas. Int. J. Remote Sens. 20, 1107—1124. https://doi.org/10.1080/014311699212876

Banks, A., Melin, F., 2015. An Assessment of Cloud Masking Schemes for Satellite Ocean Colour Data of Marine Optical Extremes. Int. J. Remote Sens. 36, 797—821. https://doi.org/10.1080/01431161.2014.1001085

Bennouna, Y.S., Curier, L., de Leeuw, G., Piazzola, J., Roebeling, R., de Valk, P., 2010. An automated day-time cloud detection technique applied to MSG-SEVIRI data over Western Europe. Int. J. Remote Sens. 31, 6073—6093. https://doi.org/10.1080/01431160903376399

Bergman, J.W., Salby, M.L., 1996. Diurnal variations of cloud cover and their relationship to climatological conditions. J. Climate 9 (11), 2802—2820. https://doi.org/10.1175/1520-0442(1996)009⟨2802:DVOCCA⟩2.0.CO;2

Bergman, J.W., Salby, M.L., 1997. The role of cloud diurnal variations in the time-mean energy budget. J. Climate 10 (5), 1114—1124. https://doi.org/10.1175/1520-0442(1997)010⟨1114:TROCDV⟩2.0.CO;2

Chepfer, H., Brogniez, H., Noel, V., 2019. Diurnal variations of cloud and relative humidity profiles across the tropics. Sci. Rep-UK 9, 16045. https://doi.org/10.1038/s41598-019-52437-6

Chepfer, H., Cesana, G., Winker, D., Getzewich, B., Vaughan, M., Liu, Z., 2013. Comparison of two different cloud climatologies derived from CALIOP attenuated backscattered measurements (Level 1): the CALIPSO-ST and the CALIPSO-GOCCP. J. Atmos. Ocean. Tech. 30, 725—744. https://doi.org/10.1175/JTECH-D-12-00057.1

Chepfer, H., Bony, S., Winker, D.M., Chiriaco, M., Dufresne, J.-L., Seze, G., 2008. Use of CALIPSO lidar observations to evaluate the cloudiness simulated by a climate model. Geophys. Res. Lett. 35, 1—6. https://doi.org/10.1029/2008GL034207

Cracknell, A.P., 1997. The Advanced Very High Resolution Radiometer AVHRR. Taylor & Francis, London, 1—556.

EUMETSAT, 01 17, 2007. Radiometric Calibration of MSG SEVIRI Level 1.5 Image Data in Equivalent Spectral Blackbody Radiance, Doc. No.: EUM/OPS-MSG/TEN/03/0064, 26. https://www.eumetsat.int

EUMETSAT, 10 25, 2012. Conversion from radiances to reflectances for SEVIRI warm channels. Description of the conversion from radiance to reflectance for the SEVIRI reflective bands (VIS06, VIS08, NIR16 and HRV), 6. http://www.eumetsat.int

Finkensieper, S., Stengel, M., Selbach, N., Hollmann, R., Werscheck, M., Meirink, F., 2018. J. ICDR SEVIRI Clouds — based on CLAAS-2 methods, Satellite Application Facility on Climate Monitoring. https://wui.cmsaf.eu

Gomis, D., Ruiz, S., Sotillo, M.G., Álvarez-Fanjul, E., Terradas, J., 2008. Low frequency Mediterranean sea level variability: The contribution of atmospheric pressure and wind, Global Planet. Change 63, 215—229. https://doi.org/10.1016/j.gloplacha.2008.06.005

Hurrell, J.W., 1995. Decadal Trends in the North Atlantic Oscillation. Science 269, 676—679. https://doi.org/10.1126/science.269.5224.676

Jakobson, E., Keernik, H., Luhamaa, A., Ohvril, H., 2014. Diurnal variability of water vapour in the Baltic Sea region according to NCEP-CFSR and BaltAn65+ reanalyses. Oceanologia 56 (2), 191—204. https://doi.org/10.5697/oc.56-2.191

Jedlovec, G., 2009. Automated detection of clouds in satellite imagery. Adv. Geosci. Remote Sens. 303—316. https://doi.org/10.5772/8326

Jędrasik, J., 2019. Modelowanie retrospektywne i prognozowanie hydrodynamiki Morza Bałtyckiego, Gdańsk, UG, 190 pp.

Jędrasik, J., Kowalewski, M., 2019. Mean annual and seasonal circulation patterns and long-term variability of currents in the Baltic Sea. J. Marine Syst. 193, 1—26. https://doi.org/10.1016/j.jmarsys.2018.12.011

Kaczmarek, S., Dera, J., 1998. Radiation flux balance of the sea-atmosphere system over the southern Baltic Sea. Oceanologia 40, 277—306.

Kowalewska-Kalkowska, H., Kowalewski, M., 2019. Combining Satellite Imagery and Numerical Modelling to Study the Occurrence of Warm Upwellings in the Southern Baltic Sea in Winter. Remote Sens.-Basel. 11 (24), 2982. https://doi.org/10.3390/rs11242982

Kowalewski, M., 1997. A three-dimensional, hydrodynamic model of the Gulf of Gdańsk. Oceanol. Stud. 26 (4), 77—98.

Krężel, A., Kozłowski, Ł., Paszkuta, M., 2008. A simple model of light transmission through the atmosphere over the Baltic Sea utilising satellite data. Oceanologia 50 (2), 125—146.

Krężel, A., Paszkuta, M., 2011. Automatic Detection of Cloud Cover over the Baltic Sea. J. Atmos. Ocean. Tech. 28, 1117—1128. https://doi.org/10.1175/JTECH-D-10-05017.1

Kriebel, K.T., Gesell, G., Kästner, M., Mannstein, H., 2003. The cloud analysis tool APOLLO: improvements and validations. Int. J. Remote Sens. 24 (12), 2389—2408. https://doi.org/10.1080/01431160210163065

Kriebel, K.T., Saunders, R.W., Gesell, G., 1989. Optical properties of clouds derived from fully cloudy AVHRR pixels. Beiträge zur Physik der Atmosphäre 62, 165—171.

Kryvobok, O., Senesi, S., Morel, C., 2005. Using Meteosat second generation high resolution visible data for the improvement of the rapid developping thunderstorm product. World Weather Research, Programme Symposium on Nowcasting and Very Short Range Forecas. Toulouse, France.

Latos, B., Lefort, T., Flatau, M.K., Flatau, P.J., Permana, D.S., Baranowski, D.B., Paski, J.A.I., Makmur, E., Sulystyo, E., Peyrillé, P., Feng, Z., Matthews, A.J., Schmidt, J.M., 2021. Equatorial Waves Triggering Extreme Rainfall and Floods in Southwest Sulawesi, Indonesia. Mon. Weather Rev. 149 (5), 1381—1401. https://doi.org/10.1175/MWR-D-20-0262.1

Lehmann, A., Krauss, W., Hinrichsen, H.-H., 2002. Effects of remote and local atmospheric forcing on circulation and upwelling in the Baltic Sea. Tellus A 54 (3), 299—316. https://doi.org/10.3402/tellusa.v54i3.12138

Li, X., Zheng, H., Han, C., Wang, H., Dong, K., Jing, Y., Zheng, W., 2020. Cloud Detection of SuperView-1 Remote Sensing Images Based on Genetic Reinforcement Learning. Remote Sens.-Basel. 12 (19), 3190. https://doi.org/10.3390/rs12193190

Mahajan, S., Fataniya, B., 2020. Cloud detection methodologies: variants and development—a review. Complex & Intelligent Systems 6, 251—261. https://doi.org/10.1007/s40747-019-00128-0

Masuda, K., Takashima, T., Takayama, Y., 1988. Emissivity of pure and sea waters for the model sea surface in the infrared window regions. Remote Sens. Environ. 24 (2), 313—329. https://doi.org/10.1016/0034-4257(88)90032-6

Paszkuta, M., Zapadka, T., Krężel, A., 2019. Assessment of cloudiness for use in environmental marine research. Int. J. Remote Sens. 40 (24), 9439—9459. https://doi.org/10.1080/01431161.2019.1633697

Platnick, S., Meyer, K., King, M.D., Wind, G., Amarasinghe, N., Marchant, B., Arnold, G.T., Zhang, Z., Hubanks, P.A., Holz, R.E., Yang, P., Ridgway, W.L., Riedi, J., 2017. The MODIS cloud optical and microphysical products: Collection 6 updates and examples from Terra and Aqua. IEEE T. Geosci. Remote 55, 502—525. https://doi.org/10.1109/TGRS.2016.2610522

Post, P., Aun, M., 2020. Changes in satellite-based cloud parameters in the Baltic Sea region during spring and summer (1982—2015). Adv. Sci. Res. 17, 219—225. https://doi.org/10.5194/asr-17-219-2020

Reuter, M., Fischer, J., 2014. A comparison of satellite-retrieved and simulated cloud coverage in the Baltic Sea area as part of the BALTIMOS project. Theor. Appl. Climatol. 118, 695—706. https://doi.org/10.1007/s00704-009-0208-8

Rozwadowska, A., 2004. Optical thickness of stratiform clouds over the Baltic inferred from on-board irradiance measurements. Atmos. Res. 72, 129—147. https://doi.org/10.1016/j.atmosres.2004.03.012

Ruiz, S.D., Gomis, M.S., Josey, S., 2008. Characterization of surface heat fluxes in the Mediterranean Sea from a 44-year high-resolution atmospheric data set, Global Planet. Change 63 (2—3), 258—274. https://doi.org/10.1016/j.gloplacha.2007.12.002

Saunders, R.W., Kriebel, K.T., 1988. An improved method for detecting clear sky and cloudy radiances from AVHRR data. Int. J. Remote Sens. 9, 123—150. https://doi.org/10.1080/01431168808954841

Wang, M., He, G., Zhang, Z., Wang, G., Wang, Z., Yin, R., Cui, S., Wu, Z., Cao, Xi., 2019. A radiance-based split-window algorithm for land surface temperature retrieval: Theory and application to MODIS data. Int. J. Appl. Earth Obs. 76, 204—217. https://doi.org/10.1016/j.jag.2018.11.015

Winker, D.M., Vaughan, M.A., Omar, A., Hu, Y., Powell, K.A., 2009. Overview of the CALIPSO mission and CALIOP dataprocessing algorithms. J. Atmos. Ocean. Tech. 26, 2310—2323. https://doi.org/10.1175/2009JTECHA1281.1

Woźniak, B., Bradtke, K., Darecki, M., Dera, J., Dudzińska-Nowak, J., Dzierzbicka-Głowacka, L., Ficek, D., Furmańczyk, K., Kowalewski, M., Krężel, A., Majchrowski, R., Ostrowska, M., Paszkuta, M., Stoń-Egiert, J., Stramska, M., Zapadka, T., 2011a. SatBaltic — a Baltic environmental satellite remote sensing system- an ongoing project in Poland. Part 1: Assumptions, scope and operating range. Oceanologia 53 (4), 897—924. https://doi.org/10.5697/oc.53-4.897

Woźniak, B., Bradtke, K., Darecki, M., Dera, J., Dudzińska-Nowak, J., Dzierzbicka-Głowacka, L., Ficek, D., Furmańczyk, K., Kowalewski, M., Krężel, A., Majchrowski, R., Ostrowska, M., Paszkuta, M., Stoń-Egiert, J., Stramska, M., Zapadka, T., 2011b. SatBaltic — a Baltic environmental satellite remote sensing system — an ongoing project in Poland. Part 2: Practical applicability and preliminary results. Oceanologia 53 (4), 925—958. https://doi.org/10.5697/oc.53-4.925

Zapadka, T., Krężel, A., Paszkuta, M., Darecki, M., 2015. Daily radiation budget of the Baltic sea surface from satellite data. Pol. Marit. Res. 22 (3), 50—56. https://doi.org/10.1515/pomr-2015-0056

Zapadka, T., Ostrowska, M., Stoltmann, D., Krężel, A., 2020. A satellite system for monitoring the radiation budget at the Baltic Sea surface. Remote Sens. Environ. 240, 11683. https://doi.org/10.1016/j.rse.2020.111683